Materials Characterization 114 (2016) 289–295

Contents lists available at ScienceDirect

Materials Characterization

journal homepage: www.elsevier.com/locate/matchar

Influence of the microstructure on the resulting 18R martensitic transformation of polycrystalline Cu—Al—Zn thin films obtained by sputtering and reactive annealing

P. Domenichini [a], A.M. Condó [a,b], F. Soldera [c], M. Sirena [a,b], N. Haberkorn [a,b,*]

[a] Instituto Balseiro, Bustillo 9500, S. C. de Bariloche, Argentina
[b] Centro Atómico Bariloche, Comisión Nacional de Energía Atómica, Av. Bustillo 9500, 8400 San Carlos de Bariloche, Argentina
[c] Department of Materials Science & Engineering, Saarland University, D-66123 Saarbruecken, Germany

ARTICLE INFO

Article history:
Received 21 January 2016
Received in revised form 10 March 2016
Accepted 12 March 2016
Available online 15 March 2016

Keywords:
Thin films
Microstructure
Shape memory

ABSTRACT

We report the influence of the microstructure on the martensitic transformation in polycrystalline Cu—Zn—Al thin films with 18R structure. The films are grown in two steps. First, Cu—Al thin films are obtained by DC sputtering. Second, the Zn is introduced in the Cu—Al thin films by the annealing them together with a bulk Cu—Zn—Al reference. The crystalline structure of the films was analyzed by X-ray diffraction and transmission electron microscopy. The martensitic transformation temperature was measured by electrical transport using conventional four probe geometry. It was observed that temperatures above 973 K are necessary for zincification of the samples to occur. The resulting martensitic transformation and its hysteresis (barrier for the transformation) depend on the grain size, topology and films thickness.

1. Introduction

Fabricating thin films based on shape memory alloys (SMAs) has been the focus of numerous studies during the last years due to potential technological applications in micro electromechanical systems (MEMS) [1] and miniature robotics [2]. Shape memory is a property associated with the capability of certain materials to return to their original shape after being deformed in a low temperature phase (martensite) and then heated to a high temperature phase (austenite). SMAs include Ni—Ti [3], Fe—Pd [4], Ni—Mn—Ga [5,6], and Cu based alloys [7,8], among others. Most of the technological applications of Ni—Ti are based on biocompatibility (including bulk and low dimensional systems) [9,10]. Systems such as Fe—Pd and Ni—Mn—Ga have potential applications based on the interplay between magnetism and shape memory [5]. Copper based alloys are particularly useful for actuator based applications in cases in which biocompatibility is not required and low-cost devices can be designed for specific purposes. Thin films of Cu-based alloys present shape memory effect [11,12]. Martensitic transformation has been reported in single crystalline Cu—Zn nanowires [13], and good potential mechanical response in Cu—Al—Ni nano pillars [14]. The martensitic transition temperature (M_s) in Cu-based alloys can be tuned in a wide range of temperature by small changes on composition [8,9]. In addition, modifying the valence electron concentration per atom (e/a) allows the stabilization of at least three different martensitic structures. Each structure presents different hysteresis width (Δh) [7,15].

The thermo cycling and the stress for the mechanically induced martensitic transformation of the different SMAs depend on the dimension [14,16,17] and the microstructure [11,12,18–20] of the samples. There are two size scales that determine the properties of SMA thin films: the grain size D and the film thickness t [11,12,18,19]. The martensitic transformation in thin films is also affected by chemical inhomogeneities [12,21], precipitates [22] and topology [23,24,23]. A notable influence of the microstructure on the martensitic transformation of Cu—Zn—Al and Cu—Al—Ni thin films grown by sputtering has been reported [11,12]. The thermal induced martensitic transformation is affected by different energies. The driving force for the transformation in given by the chemical free energy ($\Delta G^{chem} = \Delta H - T\Delta S$; being ΔH the enthalpy and ΔS the entropy). Interfacial energies and size effects increase the barrier for the transformation. The interfacial energies depend on grain boundary attained by martensite plates (γ_{gb}), the interfaces between austenite and martensite plates (γ_{am}), and the twin interfaces within martensite plates (γ_{tw}) [25].

Here, we study the resulting martensitic transformation in polycrystalline Cu—Zn—Al thin films with 18R martensitic structure. We are particularly interested in identifying possible size and disorder effects. The films are grown in two steps [11]. First, a Cu—Al film with nanometric grain size is grown by DC sputtering. Second, the film is annealed together with a Cu—Zn—Al volumetric reference. During the thermal annealing the as-grown Cu—Al film copy the Zn chemical composition of the bulk reference and the microstructure is modified due to an increment in the grain size. The chemical composition of

* Corresponding author at: Centro Atómico Bariloche, Comisión Nacional de Energía Atómica. Av. Bustillo 9500, 8400 San Carlos de Bariloche, Argentina.
E-mail address: nhaberk@cab.cnea.gov.ar (N. Haberkorn).

http://dx.doi.org/10.1016/j.matchar.2016.03.008
1044-5803/

the samples is selected in the region of ternary phase diagram of Cu—Zn—Al, which corresponds to minimum equilibrium temperature for austenite (β) phase ($e/a \approx 1.48$). The results are divided in two sections. The first one refers to the influence of the thermal annealing on the zincification process and on the resulting microstructure. The second shows the influence of the increment in the grain size on the resulting martensitic transformation (Δh and extension of the transformation). The results show that thermal annealing above 973 K is necessary for zincification of the Cu—Al thin films to occur. The time required for Zn homogenization depends on the annealing temperature. The final microstructure of annealed films is affected by the microstructure of the precursor Cu—Al. The Δh is notably reduced from 45 K (grain size ≈1 μm) to values below 25 K (grain size ≈3–7 μm). These results evidence that with an appropriate design, growth parameters and thermal annealing (tuning of M_s and Δh), Cu—Zn—Al thin films have potential applications for devices based on the memory effect [11].

2. Experimental

Binary precursor Cu—Al thin films were grown by DC sputtering. The Cu—Al targets were prepared with pure metals melted in an encapsulated quartz tube under argon atmosphere. Two different setups were used: 1- A 5.0 (0.2) μm thick Cu—Zn film was grown on Si (100) at room temperature (target with composition Cu – 19.8 *at.%* Al). 2- Two films with nominal thickness (t) of 3 μm and 6 μm were grown on highly oriented pyrolytic graphite HOPG (0001) at 823 K (Cu – 19.8 *at.%* Al). When high deposition temperature is used the lamellar structure of the HOPG (0001) permits to takes away the film from the substrate. This is not possible for films grown on Si (100) at high temperatures. During the deposition, the atmosphere was 10 mTorr of argon, the target power was 50 W and the substrates were positioned 7 cm over the target. Deposition sputtering rate was estimated from cross section scanning electron microscope (SEM) images (not shown), giving a growth rate of ~50 nm/min. The thermal annealing for each film is described in the next section. The bulk reference was prepared by considering a valence electron concentration $(e/a) = 1.48$, which corresponds to the 18R martensite structure. The M_s value was estimated according to ref. [26]. The selected chemical composition was Cu- 14.30 *at.%* Zn- 16.85 *at.%* Al ($M_s \approx 285$ K).

The Cu—Al film grown on Si (100) with no intentional heating of the substrate was easily peeled off from the substrate and cut into six different pieces. Each piece was encapsulated in quartz tubes under argon atmosphere together with a Cu—Zn—Al bulk reference for reactive annealing. Wherever used, the notation [*t-T$_a$-time*] indicates a film on Si (100) with annealing temperature T_a [K] and annealing *time* [hours]. The thermal annealing in the films was performed at the following T_a and times: 853 K and 1 h [5-853-1]; 1003 K and 1 h [5-1003-1]; 1003 K and 3 h [5-1003-3]; 1053 K and 1 h [5-1053-1]; 1123 K and 1 h [5-1123-1]; and 1123 K and 24 h [5-1123-24]. After annealing, all the samples were quenched in ice water. The films growths on HOPG (0001) were peeled off from the substrate with glue tape (removed with organic solvents) and were encapsulated in quartz tubes under argon atmosphere together with a Cu—Zn—Al bulk reference. The thermal annealing parameters were 1123 K and 1 h.

The structure of the films was studied by transmission electron microscopy (TEM) with a TEM CM200 UT and a TEM FEI Tecnai F20 UT. TEM specimens were prepared using standard ion milling techniques in a Gatan PIP system. In [H *t*-1123-1] a TEM specimen for cross section was done carried out using a focused ion beam (FIB)/SEM dual beam FEI Helios NanoLab 600 equipped with a micromanipulator Omniprobe 100. The films were characterized by X-ray diffraction (XRD) in a Panalytical Empyrean equipment using Cu K_α radiation. The roughness of the films was characterized using atomic force microscopy (AFM) with a Dimension 3100 Bruker equipment. The martensitic transformation was characterized by electrical transport using conventional four-probe geometry.

3. Results

3.1. Annealing of Cu—Al grown on Si (100)

Obtaining a ternary Cu—Al—Zn alloy with austenite structure from binary Cu—Al requires both diffusion of Zn atoms and high annealing temperatures. Research of the microstructure of Cu—Al—Zn thin films after different annealing procedures has been carried out by XRD and TEM. The thermal annealing was performed on different sections of the 5 μm Cu—Al film grown on Si (100). The lower and higher boundaries for annealing temperatures for the synthesis of ternary Cu—Zn—Al thin films are given by the stabilization of the β-phase (≈823 K for e/a ≈ 1.48) and the melting point of the binary Cu—Al alloy (≈1173 K). Fig. 1 shows the XRD obtained for the as-grown film and the pieces with different thermal annealing. The peaks corresponding to the as-grown Cu—Al film (see Fig. 1*a*) are indexed as α FCC (expected for the binary alloy at this composition [27]). The films grown textured along in the (111) axis [11,28]. Thermal annealing at 853 K (see Fig. 1*b*) produces recrystallization of the FCC films (peaks corresponding to other crystalline reflections appear). After annealing at 1003 K for 1 h (see Fig. 1*c*), peaks corresponding to the austenite phase (β-phase) are observed. To index the peaks for the β phase, an ordered $L2_1$ structure was considered. Similar XRD patterns with austenite phase were obtained for [5-730-3], [5-1053-1] and

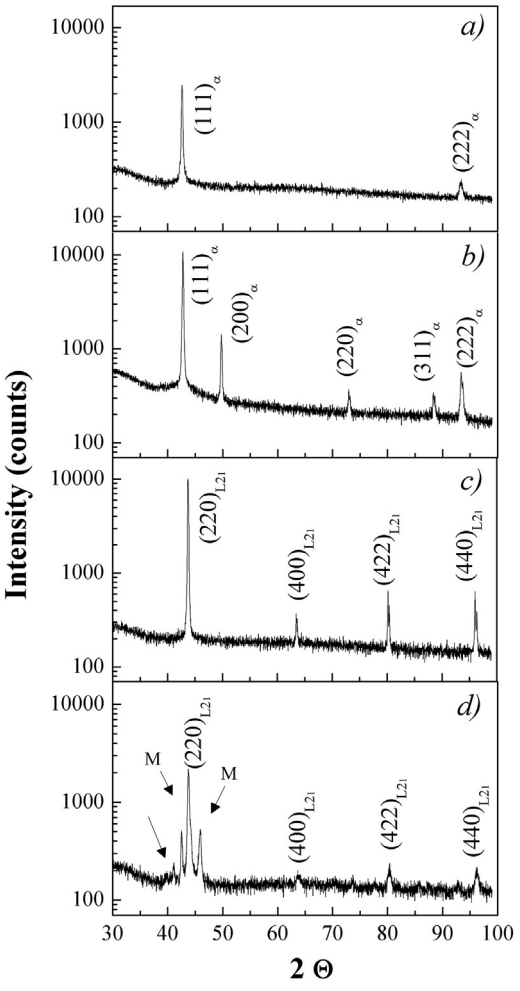

Fig. 1. X-ray diffraction patterns at room temperature of: a) As-grown Cu—Al film; b) [5-853-1]; c) [5-1003-1]; d) [5-1123-24]. The peaks were indexed by considering FCC (α-phase) and β-phase with $L2_1$ structure. M corresponds to reflexions that can be associated with martensite.

[5-1123-1]. XRD for [5-1123-24] shows coexistence of L2$_1$ and 18R martensite (see Fig. 1*d*).

Fig. 2 shows a typical bright field TEM image (for [5-1123-1]) used for built grain size histograms as function of the annealing process. The inset shows an electron diffraction pattern corresponding to the L2$_1$ structure. Fig. 3*a–d* shows the grain size histograms and the corresponding fitting with a log-normal function. The grain size mean D and the distribution width σ were obtained. Initially, the as-grown film presented small grains with mean grain diameter $D = 150$ nm (see Fig. 3*a*). After annealing at 853 K for 1 h, the grain structure of the film was relatively inhomogeneous and its size distribution could not be adjusted to a log-normal function (see Fig. 3*b*). The grain diameters range from <100 nm to 1.5 μm. No Zn was observed in [5-853-1] by EDS analyses in both TEM (see Fig. 4) and SEM specimens. The films [5-1003-1] (see Fig. 3*c*), [5-1003-3], [5-1053-1] and [5-1123-1] (see Fig. 3*d*) show a polycrystalline structure with $D \approx 1.1$ μm. EDS analysis indicates that, for every film, the Zn diffused and a ternary alloy was formed (see Fig. 4 for [5-1003-1]). No precipitates were observed, which is in agreement with XRD data. The microstructure of [5-1123-24] presented large grains with $D = 1.6$ μm ($\sigma = 0.4$).

To verify the presence/existence of martensitic transformation in the films [5-1003-1], [5-1003-3], [5-1053-1], [5-1123-1] and [5-1123-24], the related shape memory was observed when they were thermally cycled between liquid nitrogen and room temperature [11]. The transformation temperatures martensite start (M_s), martensite finish (M_f), austenite start (A_s) and austenite finish (A_f) were determined by resistance (R) vs temperature (T). Fig. 5 shows a summary of the results obtained. The curves for the as-grown film and the [5-853-1] were not included due to the absence of any structural transition. Comparing the martensitic transformations in [5-1003-1] and [5-1003-3] it is observed that $M_{s.}$ and the Δh are reduced when the annealing time is increased (Fig. 5*a* and *b*). The differences can be ascribed to the fact that the zincification process at 1003 K for 1 h is not enough for Zn homogenization. A higher $M_{s.}$ is expected for samples poorer in Zn [26]. The larger hysteresis and the large extension of the martensitic transformation ($M_f - M_s$) ≈ 75 (2) K in [5-1003-1] can be understood by considering chemical gradients. Inhomogeneities reduce the local temperature of coexistence among the two phases and increase the overcooling/overheating temperature range for the transformation/retransformation. The increment of the annealing temperature to 1073 K reduces the annealing time for Zn homogenization to 1 h. Similar $M_{s.}$ and Δh were observed in [5-1003-3], [5-1073-1] and [5-1123-1] (Fig. 5*b–d*). The $T_0 = (M_S + A_F)/2 \approx 225$ (5) K. The little differences in the $M_{s.}$ values around 200 K can be attributed to slight changes in the chemical composition of the precursor Cu—Al thin film (spatial homogeneity). It is worth mentioning that the difference between the $M_{s.}$ of these films and that expected for the target can be attributed to slight changes in the Cu—Al ratio [26]. Finally, the film [5-1123-24] presents a higher $M_{s.} \approx 280$ K and an unexpected large Δh (see Fig. 5*e*). This suggests that long annealing time produces some degradation of the films (i.e. chemical segregation of Al_2O_3 at the film surface), which is evident from a change in the metallic brightness on the surface. Therefore, this sample will be disregarded in further discussions.

The results indicate that annealing temperatures above 853 K are necessary for the zincification of Cu—Al. This temperature is determined by the zincification process and the equilibrium for the stabilization of the

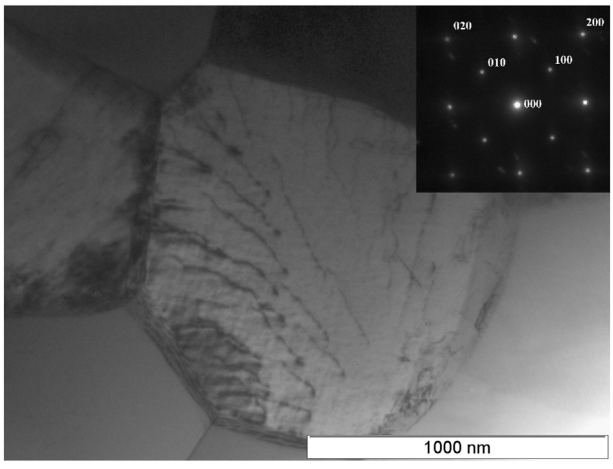

Fig. 2. Plan view bright field TEM image of a typical grain in [5-1123-1]. Inset: electron diffraction pattern corresponding to the β-phase with L2$_1$ structure. Electron diffraction pattern corresponding to the β-phase with L2$_1$ structure along the [100] zone axis. Superlattice reflexions are indicated by arrows.

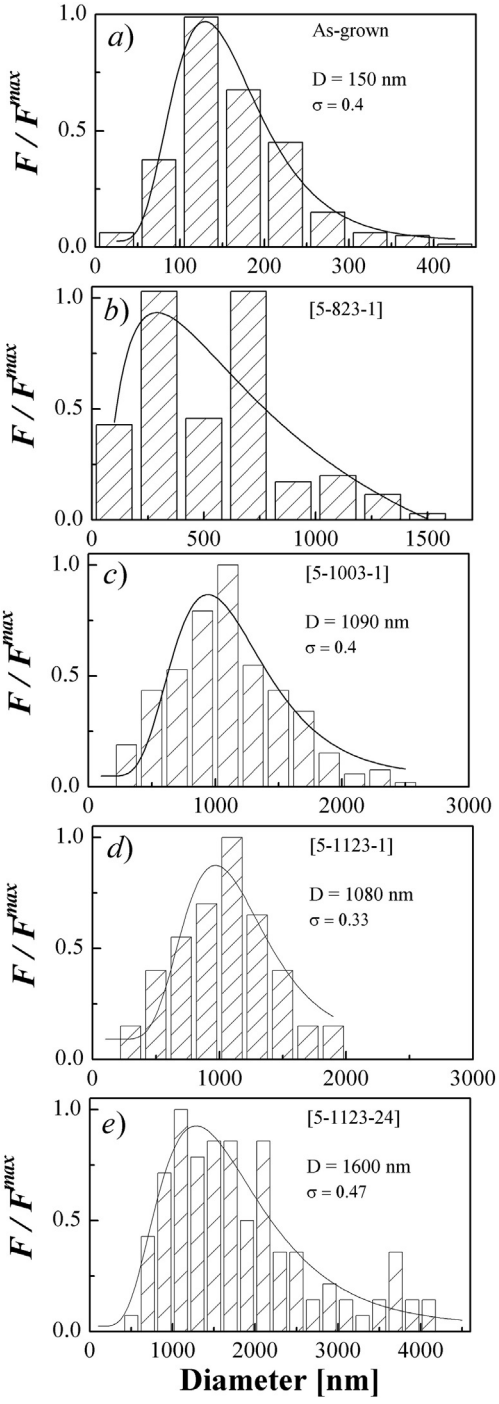

Fig. 3. Grain size histogram and its log-normal fitting of: a) As-grown Cu—Al film on Si (100); b) [5-853-1]; c) [5-1003-1]; d) [5-1123-1]; e) [5-1123-24].

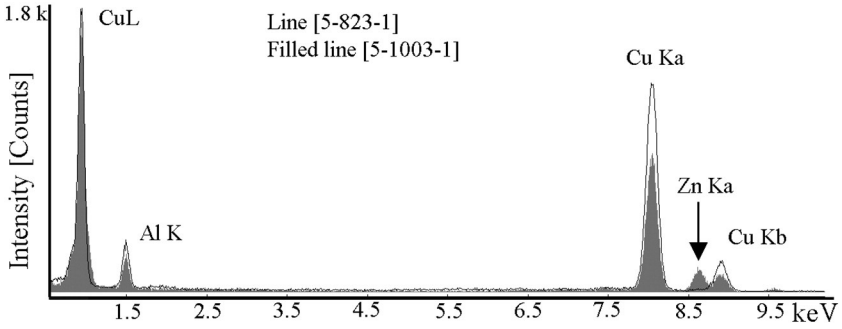

Fig. 4. Energy Dispersive spectroscopy (EDS) in the TEM of [5-853-1] and [5-1003-1].

β phase. The temperature for the zincification of Cu—Al is larger than that reported in Cu—Zn (≈723 K) [29]. The difference for zincification of Cu—Al can be associated with the surface passivation by a very thin Al_2O_3 layer, which behaves as a barrier for Zn diffusion to relatively high temperatures. The microstructure of Cu—A—Zn thin films annealed for 1 h shows $D \approx 1.1$ μm. The main changes in the grain size occur during the first steps of the recrystallization process. Long annealing time (i.e. 24 h) produces sample degradation. Although M_s can be easily modified by changing the chemical concentration of the bulk reference during the annealing [11,30], the Δh is ≈45 K. This value is much higher than that observed in bulk specimens [11].

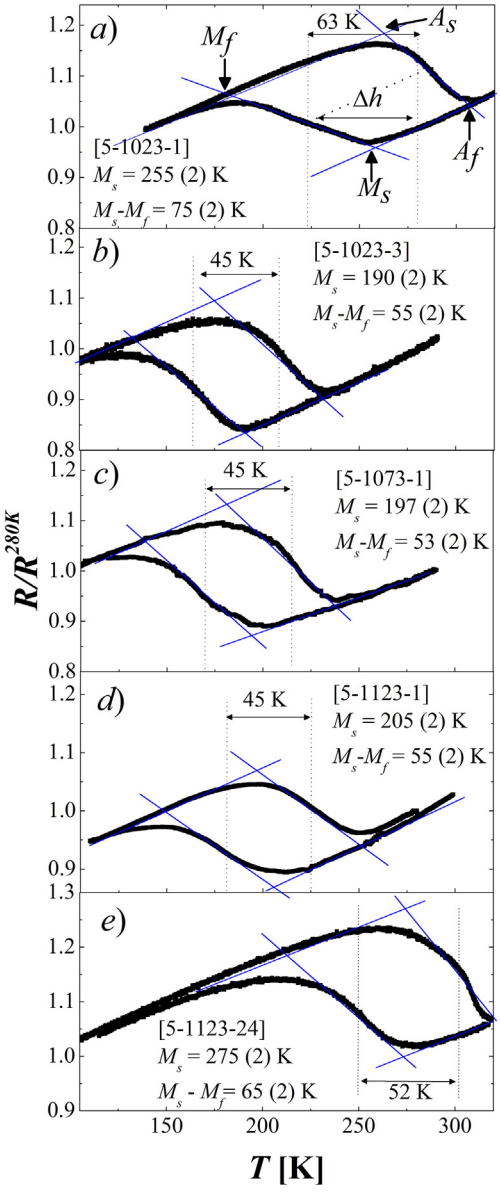

Fig. 5. Normalized resistance (R/R^{280K}) versus temperature for the different samples: a) [5-1023-1]; b) [5-1023-3]; c) [5-1053-1]; d) [5-1123-1] and e) [5-1123-24].

3.2. Annealing of Cu—Al grown on HOPG (0001)

The results discussed above indicate that Cu—Al—Zn thin films with grain size larger than $D \approx 1.1$ μm can be only obtained modifying the microstructure in the precursor Cu—Al films. This can be achieved by altering sputtering parameters such as deposition temperature. For this purpose, Cu—Al thin films at 823 K on HOPG (0001) have been grown. The main advantage of HOPG is the possibility to obtain free standing films (peeled off from the substrates) due to its laminar structure. Two films with thicknesses of 3 μm ([H 3 − 1123 − 1]) and 6 μm ([H 6-1123-1]) were obtained on HOPG (0001). For these films, a different sample holder (for temperature control) in the sputtering machine was used, which can slightly modify the distance between the target and the substrate.

The microstructure of Cu—Al—Zn thin films grown on HOPG (0001) after different annealing procedures has been studied by XRD, TEM and SEM. Initially, the as-grown Cu—Al films were not textured and presented a coexistence of α and γ-phases. The chemical concentration of the films (19.8 *at.*% Al) is close to the phase boundary (20 *at.*% Al) between α and α-γ regions in the phase diagram. The γ-phases can be understood by considering small chemical gradients that are beyond the scope of this manuscript. XRD for the two annealed films present all the peaks corresponding to the $L2_1$ phase (see Fig. 6*a*). No features of secondary phases associated with the initially present γ-phase were observed. Fig. 6*b* shows a cross section scanning TEM image in [H 3-1123-1] with three grains and their respective electron diffraction patterns. The three grains have grown with the normal of the surface along the $[110]_{L2_1}$ direction. The film present grains with size range from 3 to 7 μm (also observed in plan-view images). The sample presents one or two grains through the thickness. The EDS line scan analysis indicates that the Zn concentration is uniform across the thickness. The analysis of the bottom and top surfaces shows the presence of a thin layer of ≈20 nm of Al_2O_3. In addition, fragments of carbon (HOPG) remain at the bottom surface.

Fig. 7 shows the martensitic transformation in [H 3-1123-1] and in [H 6-1123-1] obtained from *R* vs. *T*. The T_0 value is around 255 K in both samples. The Δh is reduced from 25 K to 20 K when the film thickness is increased from 3 to 6 μm. The differences can be understood by considering the influence of the dimensionality (thickness) on the transformation. On the other hand, the $M_f - M_s$ values are reduced (≤35 K) compared to the samples with $D \approx 1.1$ μm (≈55 K).

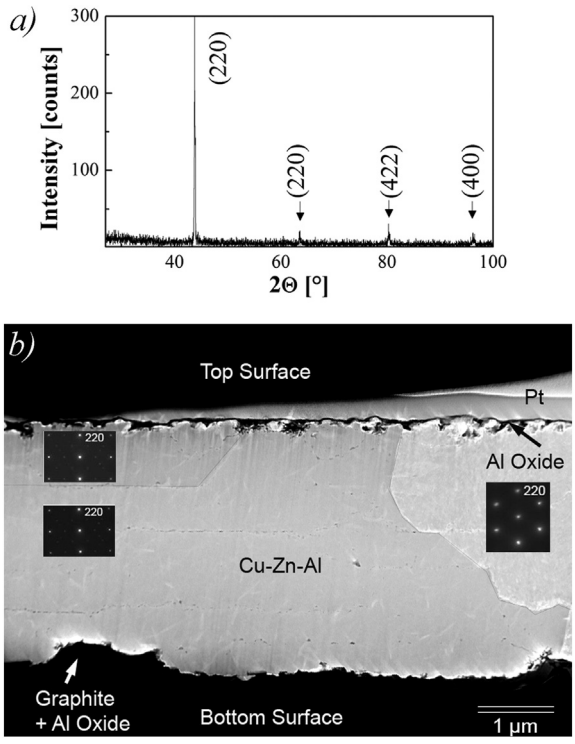

Fig. 6. *a)* X-ray diffraction patterns at room temperature of [H 6-1123-1]. *b)* Cross section TEM image in [H 3-1123-1]. The insets correspond to the electron diffraction patterns of the grains: Left and center correspond to the orientation ⟨110⟩. Right corresponds to the orientation ⟨111⟩. The direction normal to the surface is indicated.

4. Discussion

We found that Δh in Cu—Al—Zn thin films strongly depends on D and t. Cu—Al—Zn films with $D \approx 1.1$ μm and $t \approx 5$μm present a $\Delta h \approx 45$ K. For films with large grain size (3–7 μm), Δh is strongly reduced to values lower than 25 K. For 3 and 6 μm films, Δh values are 25 K and 20 K, respectively. Bulk Cu—Zn—Al with 18R structure usually presents $\Delta h \approx 4$–7 K [7]. Cu—Zn—Al melt-spun ribbons with $D \approx 13$ μm present $\Delta h \approx 10$ K, which is slightly higher than the bulk value [31]. The influence of D in Cu—Zn—Al thin films is larger than that previously observed in Cu—Al—Ni thin films with similar $L2_1 \rightarrow 18R$ transformation [12]. For example, 5 μm thick Cu—Al—Ni thin films with $D \approx 200$ nm present $\Delta h \approx 35$ K.

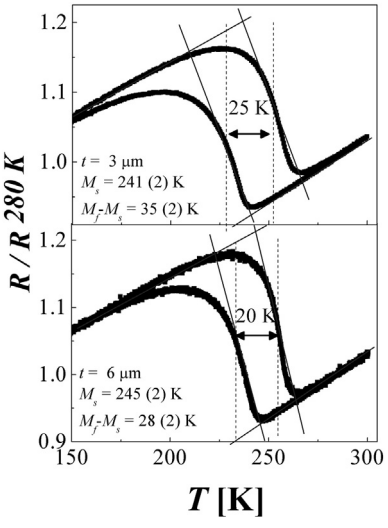

Fig. 7. Normalized resistance ($R/R^{280\ K}$) versus temperature for films grown in HOPG: *a)* [H 3-1123-1] and *b)* [H 6-1123-1].

During the martensitic transformation the change in the free energy density (i.e. unit of volume) of a sample involves different energies. During thermal cycling (without applied stress) the change in the rate of Gibbs free energy density (i.e. per unit volume) can be defined as [17]:

$$\dot{G}_{A\leftrightarrow M} = \left[\Delta G^{ch} + \gamma_i A_i + \Delta\gamma_{sf} A_{sf} + E_{el}\right]\dot{f}_M + E_{fr}\left|\dot{f}_M\right| \quad (1)$$

where $\dot{f}_M$ is the rate of martensite volume fraction ($\dot{f}_M > 0$ during forward transformation and <0 during reverse transformation). ΔG^{ch}changes of sign at T_0. $\gamma_i$is the interfacial energy (γ_{gb}, γ_{am} and γ_{tw}) per unit area and A_i is the interfacial area density. $\Delta\gamma_{sf} = \gamma_{sf}^{M} - \gamma_{sf}^{A}$ is the difference in surface energy per unit area of martensite and austenite, and multiplies the specific sample surface area A_{sf}. E_{el} is the average increment in the elastic energy density as a result of the transformation. The change in chemical energy, interfacial energy and surface energy, as well as the stored elastic strain energy due to forward transformation, are all recovered during reverse transformation, when $\dot{f}_M$ changes its sign. E_{fr} is the irreversible part of the free energy change, and is usually ascribed to frictional work produced by motion of interfaces. Following, each of these terms are briefly discussed, the magnitude of the size effect that might emerge from them is estimated, and the most plausible sources of increment of the Δh in the films are identified.

The chemical driving force ΔG^{chem} generated by undercooling around T_0 is related to the $\Delta S^{L2_1 \rightarrow 18R}$ and it can be estimated as $\partial\Delta G/\partial T = -\Delta S$ [32]. The $\Delta S^{L2_1 \rightarrow 18R}$in bulk Cu—Zn—Al ($e/a = 1.48$) is ≈ 1.46 J mol^{-1} K^{-1} $\approx -2 \times 10^5$ J K^{-1} m^{-3} [33]. The value for the energy barrier (E^T) imposed by the different mechanisms in Cu—Al—Zn bulk (with negligible contribution of dimensional effects) is $E^{T\text{-}bulk} \approx 7 \times 10^5$ J m^{-3} ($\Delta h/2 \approx 3.5$). The first contribution to be analyzed in our samples is related to interface energies due to grain size effects. In polycrystalline SMA the nucleation and growth of the martensite plates are controlled by austenite grain boundaries. The martensite plate thickness (h_{plate}) decreases as D is reduced [34]. A domain of parallel plates is usually observed in grains smaller than 10 μm [34]. Cu—Al—Zn films with $D \approx 1$ μm show $h_{plate} \approx 200$ nm [11].This h_{plate} value is beyond the predictions for bulk Cu—Al—Ni [34]. Assuming spherical grains, the total area A_{tw}^t can be calculated by the expression [35]:

$$A_{tw}^t(D,N) = \frac{\pi}{2} D^2 \left(\frac{N^2-1}{3N}\right) \quad (2)$$

where N is the number of interfaces that depends on the grain size and the h_{plate}. Using $h_{plate} = 200$ nm and $D = 1$ μm, $N = 5$ is obtained. Subsequently, A_{tw}^t depends only on D. The total interface energy per unit volume is given by:

$$E^{tw} = \gamma_{tw}\frac{A_{tw}^t}{V(D)} = \left(\frac{N^2-1}{N}\right)\frac{\gamma_{tw}}{D} \quad (3)$$

where $V(D)$ is the volume of a spherical grain. Values between 0.02 and 0.07 J m^{-2} have been reported in Cu—Al—Ni with 18R structure [25,36]. Using these values, we obtain $E^{tw\text{-}1\ \mu m} \approx 1 \times 10^5$–$3.4 \times 10^5$ J m^{-3}, which is one order magnitude smaller than $E^{T\text{-}1\ \mu m} \approx 4.5 \times 10^6$ J m^{-3}. The E^{tw} contribution to the E^T barrier of [H 3-1123-1] and [H 6-1123-1] is expected to be smaller than $E^{tw\text{-}1\ \mu m}$ [34].

Continuing the analyses, we estimate other contributions to the E^T of the films. The barrier energies estimated from $\partial T = 12.5$ K and $\partial T = 10$ K are 2.5×10^6 J m^{-3} and 2.0×10^6 J m^{-3} for [H 3-1123-1] and [H 6-1123-1], respectively. These films present similar

microstructure with 1 or 2 grains across thickness (very low density of grain boundaries). Therefore, the difference in the barrier ($\approx 5 \times 10^5$ J m^{-3}) of the films should be related to dimensional effects. Surface energies of metallic materials are usually very low, e.g. around 1–3 J m^{-2} [37]. Considering $\Delta\gamma_{sf} \leq 1$ J m^{-2} and the *surface*/volume ratio $\approx 2/t$, the $\Delta\gamma_{sf}A_i$ contributions should be 6.7×10^5 and 3.5×10^5 for [H 3-1123-1] and [H *6*-1123-1], respectively. Thus, the difference in the E^T of films grown on HOPG is mainly related to thickness effects.

The stored elastic energy during the solid-state martensitic transformation proceeds from dilatation and shear of the original austenite lattice. The change in volume and shape of a transformed region must be accommodated by its surrounding austenite or other martensite variants. The analyses for micro wires [17] and nanopilars [14] indicates that E_{el} is usually reduced when the sample size is decreased. For this reason, a little contribution of E_{el} to Δh is expected in the films.

From the analyzed results, there are several contributions to the increment in Δh of Cu—Al—Zn thin films obtained by zincification of Cu—Al films. It was found that E^{tw} has an irrelevant contribution for the barrier of our samples. The overcooling estimated by $\gamma_{tw}A_{tw}$ is smaller than 2 K in samples with $D \approx 1$ μm. The $\gamma_{gb}A_{gb}$can be roughly determined from the difference in Δh for films grown in Si (100) (with grain boundaries) and for films grown in HOPG (0001) (negligible contribution of grain boundaries). Thus, films with $D \approx 1$ μm present a $\gamma_{gb}A_{gb} \approx 2.4 \times 10^6$ J m^{-3}. The dimensional effects ($\Delta\gamma_{sf} = \gamma_{sf}^M - \gamma_{sf}^A$) are observed comparing Δh in films grown in HOPG (0001). However, the contribution of interfacial energies and dimensional effects cannot explain the $\Delta h \approx 10$ K value observed in [H *6*-1123-1]. For example, smaller contribution of the dimensionality has been observed in other systems such as Ni—Mn—Ga thin films [5] and Cu—Zn nanowires [13]. This high value of Δh of the Cu—Al—Zn thin films could be possibly ascribed to surface passivation and roughness [23,24]. As we mention above, Cu—Al—Zn thin films present a thin layer of ≈20 nm of Al_2O_3 at the surfaces. On the other hand, the thermomechanical properties of Cu-based SMA micro wires are strongly affected by surface roughness. Therefore, surface defects present an obstacle for the martensitic phase transformation (barrier increment).

For a better understanding of surface and topological barrier contributions to the martensitic transformation of our films, the sample surface of annealed films was analyzed by AFM. The histograms of peak height profile obtained from the AFM images are shown in Fig. 8. A typical AFM image for the [5-1123-1] film is included in the inset. The histograms corresponding to the as-grown Cu—Al on Si (100) and the [5-1123-1] films show that roughness is increased by the thermal annealing process from root-mean-square (rms) of 6 nm to 56 nm. For samples grown on HOPG, the influence of the thermal annealing depends on the sample surface. The bottom surface of the as-grown Cu—Al film (interface with HOPG) presented an increment in the rms from 9 nm to 170 nm which is mainly produced by the emergence of large grains on the surface. No large increment in the roughness of the top surface of the film was observed during the annealing process (rms ≈ 170 nm). The difference in the topology of the films grown on Si (100) and those grown on HOPG (0001) indicates that their contribution to the barrier could be different. On the other hand, asymmetric topologies on the bottom and top surfaces could contribute to the shape memory effects typically observed in Cu—Al—Zn films [11]. Systematic modifications of parameters, such as roughness and grain size, are necessary for a clearer understanding of their contribution to the resulting martensitic transformation in Cu—Al—Zn films.

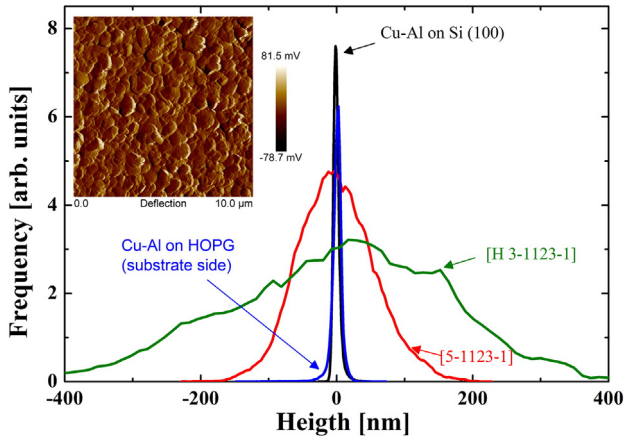

Fig. 8. Histograms of peak height profile for Cu—Al—Zn films deposited before and after thermal annealing. Inset: AFM image of a Cu—Al—Zn film obtained by thermal annealing of a Cu—Al grown in Si (100).

5. Conclusions

We have fabricated free standing Cu—Al—Zn thin films with micrometric grain size structure. The evolution of the martensitic transformation with the annealing process has been presented. As a result, we have identified possible mechanisms to increment the hysteresis of the martensitic transformation in the films. It was observed that several factors, such as grain size, thickness, dead surfaces and roughness, affect the martensitic transformation, increasing the barrier for transformation/retransformation. The Δh can be tuned from values close to 45 K to values below 25 K by modifying synthesis parameters. Understanding the influence of the dimensional, topological and microstructural mechanisms on the resulting martensitic transformation enhances potential technological applications of Cu—Zn—Al devices based on shape memory effects.

Acknowledgements

We would like to thank P. Troyon, E. Aburto, M. Isla, C. Gómez Bastida and D. Wilberger for technical assistance. This work was supported by ANPCyT PICT 2012-0884. A. M. C, M. S., and N. H. are members of CONICET (Argentina).

References

[1] Y. Fu, H. Du, W. Huang, S. Zhang, M. Hu, TiNi-based thin films in MEMS applications: a review, Sensors Actuators A 112 (2004) 395–408.
[2] J. Mohd Jani, M. Leary, A. Subic, M.A. Gibson, A review of shape memory alloy research, applications and opportunities, Mater Des 56 (2014) 1078–1113.
[3] K. Otsuka, X. Ren, Physical metallurgy of Ti–Ni-based shape memory alloys, Prog Mater Sci 50 (2005) 511–678.
[4] Yamamoto Tokujiro, Minoru Taya, Sutou Yuji, Yuanchang Liang, Wada Taishi, Sorensen Larry, Magnetic field-induced reversible variant rearrangement in Fe–Pd single crystals, Acta Mater 52 (2004) 5083–5091.
[5] V.A. Chernenko, M. Kohl, M. Ohtsuka, T. Takagi, V.A. L'vov, V.M. Kniazky, Thickness dependence of transformation characteristics of Ni–Mn–Ga thin films deposited on alumina: experiment and modelling, Mater Sci Eng A 438–440 (2006) 944–947.
[6] Backen Anja, Srinivasa R. Yeduru, Kohl Manfred, Baunack Stefan, Diestel Anett, Holzapfel Bernhard, Schultz Ludwig, Fähler Sebastian, Comparing properties of substrate-constrained and freestanding epitaxial Ni–Mn–Ga films, Acta Mater 58 (2010) 3415–3421.
[7] M. Ahlers, Martensite and equilibrium phases in CuZn and CuZnAl alloys, Prog. Mater. Sci. 30 (1986) 135–186.
[8] K. Otsuka, H. Sakamoto, K. Shimizu, Successive stress-induced martensitic transformations and associated transformation pseudoelasticity in Cu–Al–Ni alloys, Acta Metall Mater 27 (1979) 585–601.
[9] T. Duerig, A. Pelton, D. Stöckel, An overview of nitinol medical applications, Mater Sci Eng A 273–275 (1999) 149–160.
[10] Y. Fu, H. Du, W. Huang, S. Zhang, M. Hu, TiNi-based thin films in MEMS applications: a review, Sensors Actuators A Phys 112 (2004) 395–408.
[11] N. Haberkorn, F.C. Lovey, A.M. Condó, J. Guimpel, Development and characterization of shape memory Cu–Zn–Al thin films, Mater Sci Eng B 70 (2010) 5–8.
[12] C. Espinoza Torres, A.M. Condó, N. Haberkorn, E. Zelaya, D. Schryvers, J. Guimpel, F.C. Lovey, Structures in textured Cu–Al–Ni shape memory thin films grown by sputtering, Mater Charact 96 (2014) 256–262.
[13] N. Haberkorn, A.M. Condó, M. Sirena, F. Soldera, F.C. Lovey, Single crystalline β phase Cu–Zn nanowires: synthesis and martensitic transformation, Mater Lett 124 (2014) 256–260.

[14] J. San Juan, M.L. Nó, C.A. Schuh, Superelastic cycling of Cu–Al–Ni shape memory alloy micropillars, Acta Mater 60 (2012) 4093–4106.
[15] M. Ahlers, J.L. Pelegrina, The martensitic phases and their stability in CuZn and CuZnAl alloys-II. The transformation between the close packed martensitic phases, Acta Metall. Mater. 40 (1992) 3213–3220.
[16] C.P. Frick, S. Orso, E. Arzt, Loss of pseudoelasticity in nickel–titanium sub-micron compression pillars, Acta Mater 55 (2007) 3845–3855.
[17] Y. Chen, C.A. Schuh, Size effects in shape memory alloy microwires, Acta Mater 59 (2011) 537–553.
[18] T. Waitz, W. Pranger, T. Antretter, F.D. Fischer, H.P. Karnthaler, Competing accommodation mechanisms of the martensite in nanocrystalline NiTi shape memory alloys, Mater Sci Eng A 481–482 (2008) 479–483.
[19] T. Lehnert, H. Grimmer, P. Böni, M. Horisberger, R. Gotthard, Characterization of shape-memory alloy thin films made up from sputter-deposited Ni/Ti multilayers, Acta Mater 48 (2000) 4065.
[20] A. Ishida, M. Sato, Microstructure and shape memory behaviour of annealed $Ti_{51.5}Ni_{(48.5\ -\ x)}Cu_x$ (x = 6.5–20.9) thin films, Philos. Mag. 87 (2007) 5523–5538.
[21] P. Machain, A.M. Condó, P. Domenichini, G. Pozo López, M. Sirena, V.F. Correa, N. Haberkorn, Martensitic transformation in as-grown and annealed near-stoichiometric epitaxial Ni_2MnGa thin films, Philos. Mag. 95 (2015) 2527–2538.
[22] F.C. Lovey, V. Torra, Shape memory in Cu-based alloys: phenomenological behavior at the mesoscale level and interaction of martensitic transformation with structural defects in Cu–Zn–Al, Prog. Mater. Sci. 44 (1999) 189–289.
[23] S.M. Ueland, C.A. Schuh, Transition from many domain to single domain martensite morphology in small-scale shape memory alloys, Acta Mater 61 (2013) 5618–5625.
[24] M. Ueland Stian, Christopher A. Schuh, Surface roughness-controlled superelastic hysteresis in shape memory microwires, Scr Mater 82 (2014) 1–4.
[25] H. Petryk, S. Stupkiewicz, G. Maciejewski, Interfacial energy and dissipation in martensitic phase transformations. Part II: Size effects in pseudoelasticity, J Mech Phys Solids 58 (2010) 373–389.
[26] J.L. Pelegrina, M. Ahlers, The martensitic phases and their stability in CuZn and CuZnAl alloys-I. The transformation between the high temperature β phase and the 18R martensite, Acta Metall. Mater. 40 (1992) 3205–3211.
[27] J.L. Murray, The aluminum-copper system, Int Met Rev 30 (1985) 211–233.
[28] N. Haberkorn, A.M. Condó, C. Espinoza, S. Jaureguizahar, J. Guimpel, F.C. Lovey, Bulk-like behavior in the temperature driven martensitic transformation of Cu–Zn–Al thin films with 2H structure, J Alloys Compd 591 (2014) 263–267.
[29] H.E. Troiani, J.L. Pelegrina, M. Ahlers, The dezincification of α-Cu–Zn, Phys Status Solidi (a) 156 (1996) 93–106.
[30] N. Haberkorn, M. Ahlers, F.C. Lovey, Tuning of the martensitic transformation temperature in Cu–Zn thin films by control of zinc vapor pressure during annealing, Scr Mater 61 (2009) 821–824.
[31] J.L. Pelegrina, L.M. Fabietti, A.M. Condó, G. Pozo López, S.E. Urreta, The influence of microstructure on the martensitic transformation in Cu–Zn–Al melt-spun ribbons, Philos Mag 90 (2010) 2793–2805.
[32] Chen Ying, Christopher A. Schuh, A coupled kinetic Monte Carlo—finite element mesoscale model for thermoelastic martensitic phase transformations in shape memory alloys, Acta Mater 83 (2015) 431–447.
[33] R. Romero, J.L. Pelegrina, Change of entropy in the martensitic transformation and its dependence in Cu-based shape memory alloys, Mater Sci Eng A 354 (2003) 243–250.
[34] P. La Roca, L. Isola, Ph. Vermaut, J. Malarria, Relationship between martensitic plate size and austenitic grain size in martensitic transformations, Appl Phys Lett 106 (2015) 221903–221906.
[35] T. Waitz, T. Antreteer, D.F. Fischer, N.K. Simha, Size effects on the martensitic phase transformation of NiTi nanograins, J. Mech. Phys. Solids 55 (2007) 419–444.
[36] D. Shilo, A. Mendelovich, V. Novak, Investigation of twin boundary thickness and energy in CuAlNi shape memory alloy, Appl Phys Lett 90 (2007) 193113–193115.
[37] X. Wang, Y. Jia, Q. Yao, F. Wang, J. Ma, X. Hu, The calculation of the surface energy of high-index surfaces in metals at zero temperature, Surf Sci 551 (2004) 179–188.